Achim Schweikard · Floris Ernst

Medical Robotics

Springer

Medical Robotics

Achim Schweikard • Floris Ernst

Medical Robotics

Springer

Achim Schweikard
Institute for Robotics
and Cognitive Systems
University of Lübeck
Lübeck, Germany

Floris Ernst
Institute for Robotics
and Cognitive Systems
University of Lübeck
Lübeck, Germany

ISBN 978-3-319-22890-7 ISBN 978-3-319-22891-4 (eBook)
DOI 10.1007/978-3-319-22891-4

Library of Congress Control Number: 2015947502

Springer Cham Heidelberg New York Dordrecht London

Printed on acid-free paper

Springer International Publishing AG Switzerland is part of Springer Science+Business Media (www.springer.com)

Preface

Medical robotics is an interdisciplinary field, with methods from computer science, mathematics, mechanical engineering, and medicine. The field emerged in the 1980s as a new branch of robotics. Robotics itself was then a branch of artificial intelligence. However, a number of technical and mathematical problems had to be solved to bring robots to routine clinical use. These problems were far outside the scope of artificial intelligence, and this supported the emergence of the new field.

When comparing medical robotics to industrial robotics, we see that the latter field is the one that sells most robots. By contrast, some of the most challenging research problems arise in medical robotics: there is a need for improving the accuracy of surgical procedures, and image guidance has become a central element of this. If we imagine that robotic exoskeletons can help paralyzed patients, it becomes clear that we will need methods for motion learning and brain-computer interfaces.
We wrote this book as a textbook for a one-semester class on medical robotics. When writing this book, we were guided by two thoughts:

- Computer scientists and engineers should learn to understand application domains, and medicine is an ideal application domain for this purpose.
- The book should be suitable as a first course in robotics.

Comparing to standard textbooks on robotics, four elements have been added here: (1) seven-joint robots; (2) navigation, calibration, and registration; (3) connection to machine learning; and (4) applications in surgical robotics, rehabilitation robotics, and neuroengineering. The text relies entirely on the most elementary mathematical tools, and we give a detailed introduction for each new method. At the end of each chapter, we provide exercises, preparing the grounds for the tools in the next chapters, while linking to the methods in the current chapter.
Chapter 1 introduces the main applications of medical robotics.
Chapter 2 presents basic methods for describing position and orientation as well as forward robot kinematics. This includes matrices, angles, and the analysis of simple linkages.
Chapter 3 introduces inverse kinematics for robots. We develop the inverse kinematics for a seven-joint lightweight robot, called the DLR-Kuka arm. This robot is designed for applications requiring direct interaction with an operator. To obtain an inverse solution, we first solve the kinematic equations for a standard six-joint robot with revolute joints, called the elbow manipulator with spherical wrist. We obtain a building-block strategy with which common types of robots can be analyzed.
Geometric methods for inverse kinematics are an alternative to algebraic methods. We illustrate geometric methods for the kinematic analysis of common medical devices.
In Chap. 4, we consider Jacobi-matrices. There are two types of Jacobians: the analytic Jacobian and the geometric Jacobian. The analytic Jacobian offers alternative methods for the inverse analysis of robots. The geometric Jacobian is a basic tool for velocity kinematics and for analyzing the relationship between joint torques and static forces/torques acting at the tool. We apply the geometric Jacobian to problems involving C-arm X-ray imaging and robot design.
Chapter 5 establishes a connection to the classical tools from medical imaging, i.e., MR, CT, ultrasound, and X-ray imaging. With this tool set, we address several problems, such as navigation, registration, image calibration, and robotic hand-eye calibration.
Chapter 6 describes methods for treatment planning. Computer programs have been used for treatment planning in radiation oncology since the 1950s. Until the 1990s, conventional systems for radiation

oncology irradiated tumors from a small set of beam directions (typically three to five directions). To move the beam source, five-joint mechanisms with revolute and prismatic joints were used. This changed with the introduction of robotic radiosurgery. Up to 1000 distinct directions can now be used in a single treatment. This greatly increased the complexity of treatment planning.

Chapter 7 is the first chapter (in a series of three chapters) with basic methods from machine learning. We address the problem of tracking anatomical motion (heartbeat, respiration) with a robot. To this end, we learn the motion of a difficult-to-image anatomical target via the motion of a surrogate.

In Chap. 8, we predict respiratory motion to compensate for the time lag of the robot, while tracking a target. Again, machine learning is one of the main elements. In addition, we need a connection to basic methods from signal processing.

In Chap. 9, we consider motion replication. Robots for motion replication are the most commonly used surgical robots. The surgeon moves a passive robot, and thereby issues motion commands to a small replicator robot. We apply tools from machine learning to classify different types of motions, i.e., intended motion, tremor, and noise. In the replication process, we must separate these types of motions (all of which are part of the motion signal). In the same context, we apply the geometric Jacobian to the analysis of static forces and torques.

The three applications in Chaps. 7–9 all converge to a set of methods, which we term "motion learning." Humans learn motion, and it is obvious that we need dedicated tools for motion learning not only in medical robotics.

Chapter 10 discusses integrated systems in medical robotics. The methods developed in Chaps. 1–9 are the building blocks for such systems. It should be noted that the methods in Chaps. 1–9 have already found their way to the clinic, and have become routine tools, especially in oncology, but also in orthopedics and neurology, most of them via the connection to medical imaging and motion learning.

Chapter 11 gives an overview of methods for neuroprosthetics, brain-machine interfaces, and rehabilitation robotics.

In the appendix, we derive the geometric Jacobian matrix for the six-joint elbow manipulator and for the DLR-Kuka seven-joint robot. We also include solutions to selected exercises.

Additional material is available at https://medrob-book.rob.uni-luebeck.de.

Acknowledgements

We thank Max Wattenberg for converting many of the drawings to TikZ-format, Robert Dürichen for implementing several of the methods for motion prediction and for discussions on the subject, Ulrich Hofmann and Christian Wilde for their help with writing the text on brain-machine interfaces, Ivo Kuhlemann for his help with implementing and testing inverse kinematics algorithms, and Cornelia Rieckhoff for proof-reading.
We offer special thanks to Rainer Burgkart for discussions and suggestions on orthopedic navigation, John R. Adler for many discussions on navigation in neurosurgery and radiosurgery, and our doctoral students Norbert Binder, Christoph Bodensteiner, Christian Brack, Ralf Bruder, Markus Finke, Heiko Gottschling, Max Heinig, Robert Hanne, Matthias Hilbig, Philip Jauer, Volker Martens, Lars Matthäus, Christoph Metzner, Lukas Ramrath, Lars Richter, Stefan Riesner, Michael Roth, Alexander Schlaefer, Stefan Schlichting, Fabian Schwarzer, Birgit Stender, Patrick Stüber, Benjamin Wagner, and Tobias Wissel for their help with experiments and graphics and for reading drafts of the book.
Finally, we thank Mohan Bodduluri, Gregg Glosser, and James Wang for their help with implementing robotic respiration tracking and treatment planning for a clinical standard system.

Lübeck, Germany

Achim Schweikard
Floris Ernst

Contents

Chapter 1
Introduction

Robots are now used in many clinical sub-domains, for example: neurosurgery, orthopedic surgery, dental surgery, eye surgery, ear-nose and throat surgery, abdominal surgery/laparoscopy, and radiosurgery. This gives rise to a large number of new methods. However, medical robotics is not limited to surgery. In recent years, four main types of medical robots have emerged:

1. Robots for Navigation. The surgical instrument is moved by a robot arm. This allows precise positioning, based on pre-operative imaging. The motion of anatomic structures (e.g. caused by respiration and pulsation) can be tracked.
2. Robots for Motion Replication. The robot replicates the surgeon's hand motion, via a passive robotic interface. Thus we can downscale the motion, reduce tremor and improve minimally invasive methods.
3. Robots for Imaging. An imaging device is mounted to a robotic arm, to acquire 2D or 3D images.
4. Rehabilitation and Prosthetics. Mechatronic devices can support the recovery process of stroke patients. Robotic exoskeletons controlled by brain-computer interfaces can replace or support damaged anatomical structures.

We will discuss basic methods for each of the four cases. In the following section, we will begin by looking at several examples for surgical navigation.

A. Schweikard, F. Ernst, *Medical Robotics*,
DOI 10.1007/978-3-319-22891-4_1

1.1 Robots for Navigation

A first example of a medical robot is shown in Fig. 1.1. A robot guides a surgical saw. Before the intervention, the surgeon defines a cutting plane for a bone cut. During the operation, the robot places the saw in the predefined plane, and the surgeon can move the saw within this plane. This restricts the motion of the saw, and allows for placing the cuts with high precision.
In the figure, we see two types of robot joints: revolute joints and prismatic joints. For a revolute joint, a rigid link rotates about an axis. A prismatic link slides along a translational axis. The last joint in Fig. 1.1 is a prismatic joint. Here, the prismatic joint is passive, i.e. it is not actuated by a motor. Thus, the surgeon moves the saw by hand, while the motion plane is given by the robot.

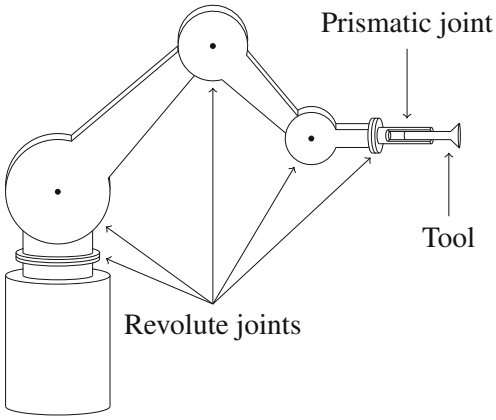

Fig. 1.1: Surgical saw mounted to a robotic arm. The arm itself consists of revolute joints. The saw is mounted to a passive component (prismatic joint). The surgeon moves the saw manually (sliding motion only). By construction, the manual motion of the saw is restricted to a single axis [6]

Remark 1.1

Fig. 1.2 illustrates a schematic notation for jointed mechanisms, for the robot in Fig. 1.1. Revolute joints are denoted by cylinders, where

the cylinder axis specifies the axis of rotation. Prismatic joints are denoted by boxes. The lid of the box indicates the direction of motion.

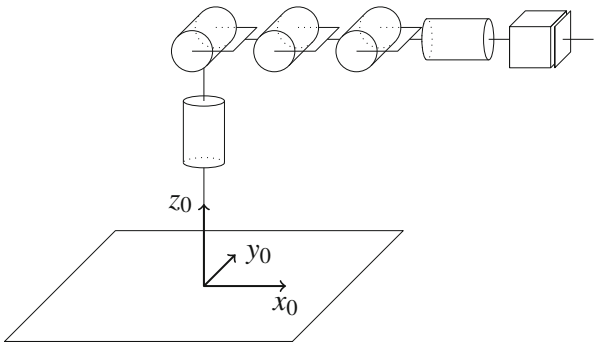

Fig. 1.2: Schematic notation for the robot in Fig. 1.1

In the figure, notice that the first two joint axes (revolute joints) intersect in space. Furthermore, the axes of joints two, three and four are parallel. We also see the axes x_0, y_0 and z_0 of a *base coordinate system*.

(End of Remark 1.1)

1.1.1 Navigation for Orthopedic Surgery

We will now show several examples for navigation problems arising in orthopedic surgery.
Figure 1.3 shows a femur bone. The region shown with the dashed pattern is the target area (e.g. a tumor). The instrument for removing the tumor is a surgical drill. The skin cut is made on the right side (an arrow indicates the drilling direction). The target is on the left side. The tumor is well visible in the CT image, but often not visible in an X-ray image. To remove the tumor, we must guide the drill. Notice also that the drill must not penetrate the joint surface. Here, the pre-operative 3D images must be matched to the intra-operative situation.
Figure 1.4 shows the head of a femur bone. A small gap between the head and the rest of the bone is visible (see arrow). Epiphyseolysis is

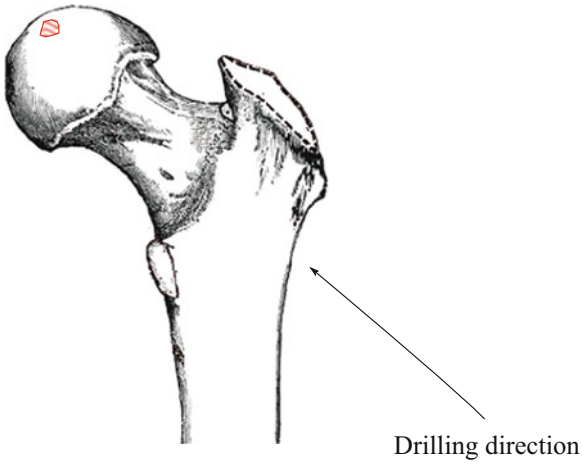

Fig. 1.3: Navigating a surgical drill. Femur figure from [3, Fig. 245]

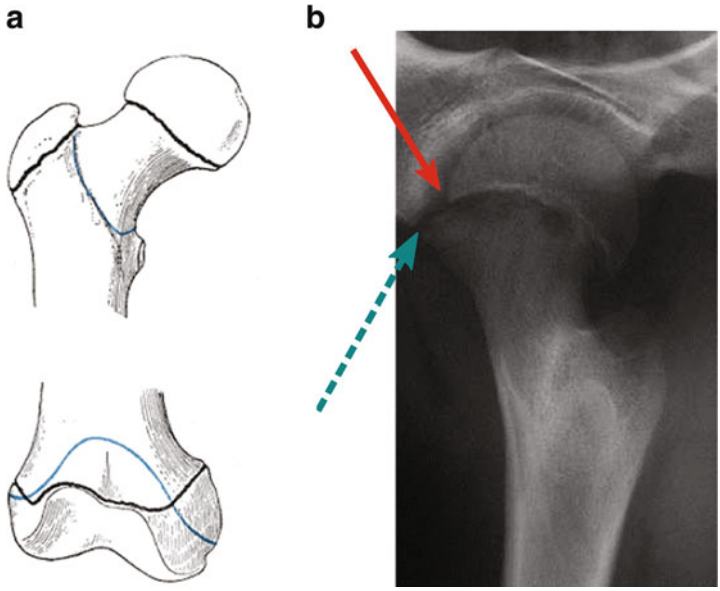

Fig. 1.4: Epiphyseolysis. *Left images*: epiphysial lines of the femur. *Source*: [3, Fig. 253]. *Right image*: X-ray image of epiphyseolysis. The femur bone is displaced against the head, the tips of the two arrows should coincide. (**a**) Epiphysial lines of the femur, shown in black. *Source*: [3, Fig. 253]. (**b**) X-ray of the femur, showing the epiphysial line at the femur head (*solid arrow*)

a condition, in which a fracture along this gap results in a downward slippage of the femur head (Fig. 1.4) [7].

Fig. 1.5: Treatment of epiphyseolysis

To stabilize the femur head, screws are used (Fig. 1.5). However, placing the screws is difficult. The reason is that only the surface of the bone consists of hard material, the *cortical bone*. The interior of the bone, called *cancellous bone*, or spongy bone, is much softer. The screw tip must reach (but not penetrate) the cortical bone surface.
Figure 1.6 shows a cross-section (slice) of a CT-data set, side-by-side with the corresponding MRI slice. The cortical bone is visible as a ring (white/light grey in the CT image, and black in the MRI data). The spongy bone is inside this ring. When placing a screw (as in Fig. 1.5), the tip of the screw should reach, but not penetrate the thin cortical bone layer.

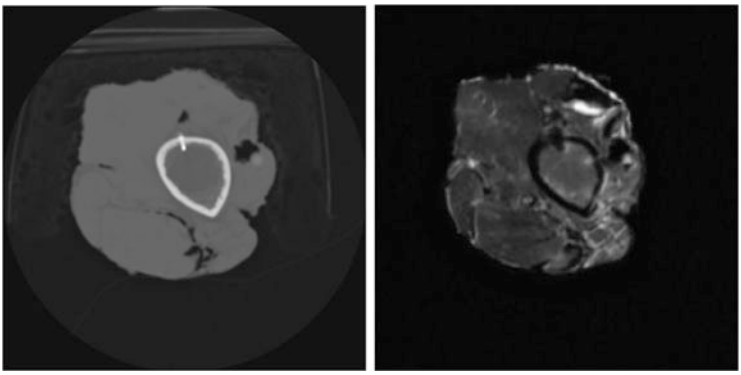

Fig. 1.6: Cortical bone and spongy bone in CT (*left*) and MRI (*right*). In the CT scan, the cortical bone shows up white (black in MRI). The spongy bone is inside

Figure 1.7 shows a similar application in spine surgery. Two or more vertebrae must be stabilized. Screws through the pedicle hold a fixation plate. Likewise, in dental surgery, implants are held by screws in delicate bony structures of the chin.
In Fig. 1.8, a wedge of the bone must be removed to obtain a better positioning of the bone axis. The navigation system guides the surgeon to locate the cutting planes during the operation.

1.1.2 Radiologic Navigation

During an intervention, the visibility of anatomic target structures is often limited. Thus, for example, a CT image is taken before an operation. During the actual operation, only X-ray imaging is available. The CT image shows more detail than an intraoperative X-ray image, but does not show the current position of the surgical instrument. For precise navigation, we would need a CT image showing *both* the instrument and the target at the same time. Thus, we need a virtual marker visualizing the instrument position in the CT image.
One first method for surgical navigation is called *radiologic navigation*. Radiologic navigation is based on X-ray imaging. During the operation, X-ray images are taken with a *C-arm* (Fig. 1.9). A C-arm is a

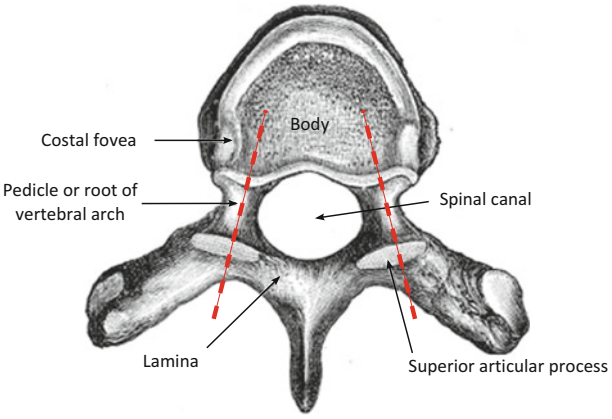

Fig. 1.7: Placement of pedicle screws. The insertion path for the screws (*dashed lines*) must not touch the spinal canal. Source of drawing [3, Fig. 82]

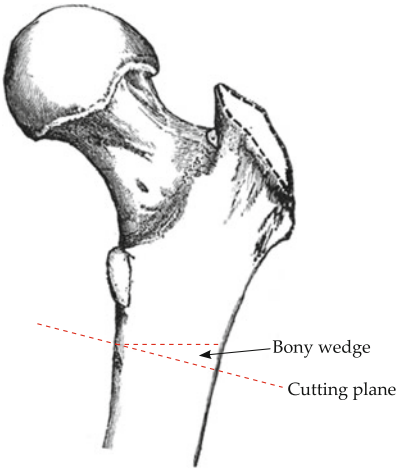

Fig. 1.8: Corrective osteotomy for the femur bone. Source of the drawing: [3, Fig. 245]

mobile X-ray imaging device with five joints. There are two prismatic joints, and three revolute joints. A C-arm allows for taking X-ray images from varying angles during an operation.
Figure 1.10 shows the joints of a C-arm, in the notation introduced in Remark 1.1.

Fig. 1.9: C-arm X-ray imaging. A C-shaped structure carries an X-ray source and an X-ray detector. The C is mounted to a jointed mechanism with five joints [2]

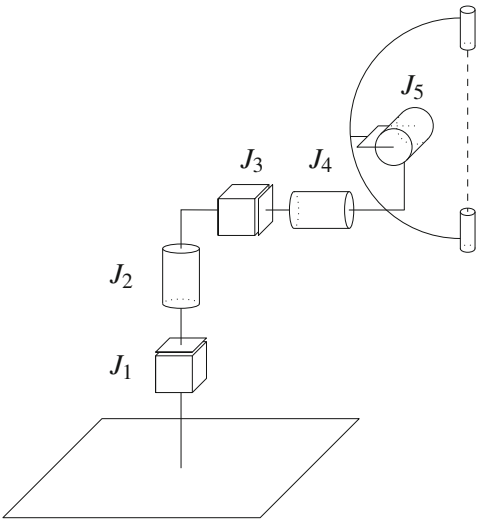

Fig. 1.10: Joints of a C-arm. J_2, J_4 and J_5 are revolute joints. J_1 and J_3 are prismatic

A second tool needed for radiological navigation is *infrared tracking* (IR tracking). An infrared tracking system consists of a camera, and one or more infrared markers, either reflective (i.e. illuminated by the camera) or active IR-LEDs (Fig. 1.11). The system tracks positions and orientations of the markers in space. Markers can be attached to objects and tools in the operating room. The camera of the tracking system is attached to the wall of the operating room, and provides the *base coordinate system*. Notice that infrared tracking not only outputs the *position* of the pointer tip of the marker, but also the *orientation* of the marker in space. This means we not only know the tip coordinates (e.g. as x-, y-, z-coordinates) with respect to the camera coordinate system, but we also obtain information about the angle and the pointing direction of the marker in space. To output such angular information, standard tracking systems use *matrices* or *quaternions*. Typical systems report the marker position to within 0.1 mm.

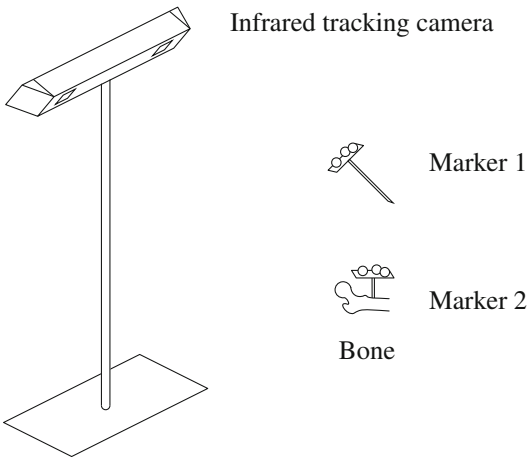

Fig. 1.11: Infrared tracking system with two markers. One of the markers is attached to a bone

Figure 1.12 shows the principle of radiological navigation. A first marker of the infrared tracking system is attached to the C-arm. The second marker is attached to the saw. After making a skin incision (opening the skin), a third marker is rigidly attached to the bone. Then an X-ray image of the bone is taken with the C-arm. Given the position

of the C-arm in space, we can compute the exact spatial coordinates of points on the bone visible in the C-arm image. These coordinates are computed with respect to the (infrared) camera coordinate system. We can now steer the robot to a predefined point on the bone surface, or guide the robot to find a pre-planned angle with respect to the bone. If the bone moves during the procedure, we can calculate and correct the displacement by subtraction.

When attaching a marker to the robot or the saw, we do not know the spatial reference between the robot's coordinate system, and the internal coordinate system of the infrared tracking camera. The process of finding the spatial mapping between the two coordinate systems is called *hand-eye calibration*. A similar problem occurs when calibrating C-arm images with respect to the infrared marker.

As noted above, tumors are often not visible in X-ray images, but well visible in 3D CT images taken before the operation. The navigation problem is now to align the bone in the X-ray image to the same bone in the CT image. The alignment should be done such that the two images match, i.e. corresponding structures should be at the same position. This process is called *image registration*. Not only X-ray images are registered to CT images, but any pair of image modalities (CT, MRI, ultrasound and many other modalities) can be considered in this context.

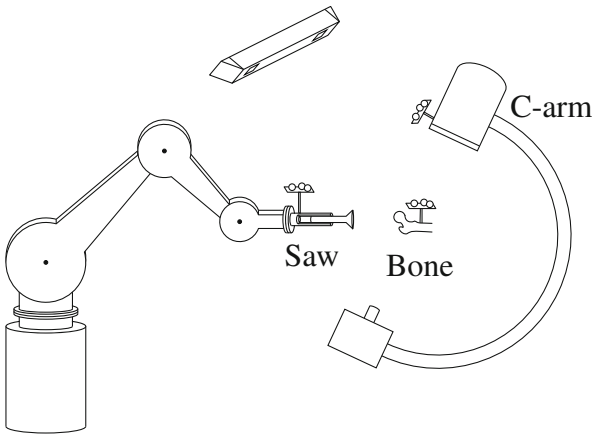

Fig. 1.12: Radiologic navigation. Markers for the infrared tracking system are attached to the saw, the C-arm and the bone

1.1.3 Stereotaxic Navigation

A second method for navigation is *stereotaxic navigation*. It is typically used in neurosurgery and allows for reaching targets in the brain with high precision.

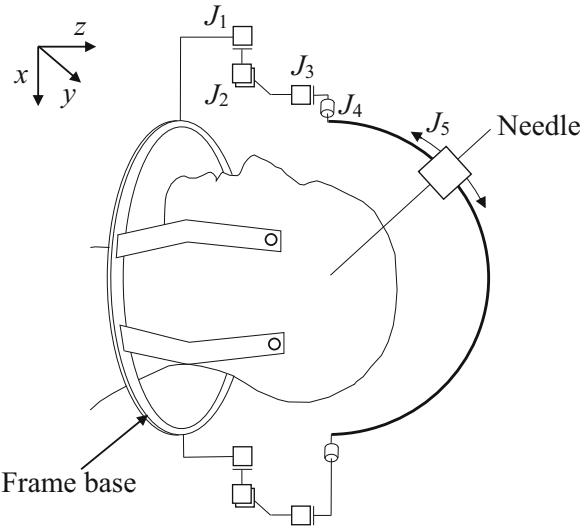

Fig. 1.13: Five-joint mechanism for stereotaxic neurosurgery

To this end, a small robotic mechanism with five joints is rigidly attached to the head of the patient (Fig. 1.13). The instrument is a needle, and can be moved by changing the settings of the joint angles. Recall the schematic notation for robot joints. In the figure, the joints are called $J_1, J_2, \ldots, J_5$. Here, J_1, J_2 and J_3 are prismatic, and J_4, J_5 are revolute joints.

During the procedure, the patient's head is fixed in space with a stereotaxic frame (Fig. 1.14). The frame has three parts (A, B and C). Part A is the frame base. This part directly attaches to the head. Part B is a box with localizers for CT/MR imaging, and attaches to the base. The localizers are also called *fiducials*. Part C is the passive jointed mechanism in Fig. 1.13, and part C can also be rigidly attached to the frame base. To this end, we remove the localizer frame B.

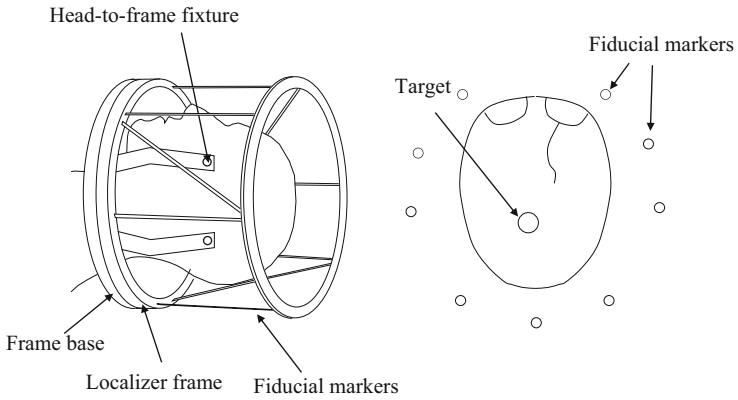

Fig. 1.14: Stereotaxic navigation in neurosurgery. The fiducial markers are visible in the CT image and provide a reference coordinate system

Figure 1.14 (left side) shows the frame base with the localizer box attached. The localizer box contains three *N*-shaped arrangements of rods. Six of these rods are horizontal, and three of them are oblique (see figure).

After taking a CT or an MR image (with the frame and localizers in place), we see vertical cross sections of the head (Fig. 1.14, right).

Vertical cross sections (with the patient on the treatment table, as in Fig. 1.14) are also called axial cross sections. The three viewing directions for imaging are shown in Fig. 1.15.

In the cross-sections, we will see points (indicated as small circles in Fig. 1.14, right), stemming from the fiducial rods. From the distance between two adjacent points (one from an oblique rod and one from a horizontal rod) we derive the z-coordinate of the image cross-section. With similar methods, we can obtain x- and y-coordinates of the target in the image.

In the next step of the procedure, we remove the localizer box with the fiducial rods, and attach the jointed mechanism to the frame base. As noted above, the jointed mechanism carries the instrument (e.g. a biopsy needle or an electrode).

Having determined the coordinates of the target in the images, we can compute the angle settings for the jointed mechanism and insert a

needle along a predefined path. Again, calibration methods are needed to map the CT/MR coordinate system to the frame coordinate system.

Example 1.1

The joints J_4 and J_5 in Fig. 1.13 are revolute joints. The joint angles of J_4 and J_5 determine the orientation of the needle. The needle tip moves when we change the values of the angles. Let θ_4 and θ_5 be the values of the joint angles for J_4 and J_5. The current values for θ_4 and θ_5 can be read from a scale imprinted onto the metal frame. We can compute the position of the needle tip for given θ_4, θ_5. The position is described with respect to the coordinate system shown in the figure. We can also derive a closed form expression, stating the coordinates of the needle tip as a function of θ_4, θ_5. Similarly, we can include the prismatic joints into the computation. This derivation of a closed formula is one example of a *forward kinematic analysis* of a mechanism. Conversely, computing angle values from a given tip position and needle orientation is called an *inverse kinematic analysis* (see also Exercise 1.1 at the end of this chapter).

(End of Example 1.1)

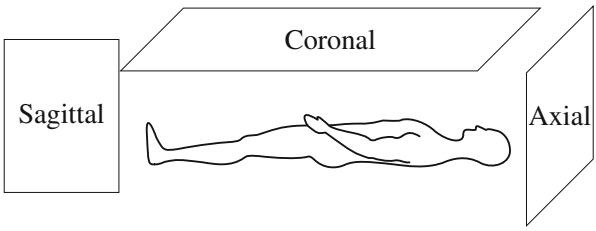

Fig. 1.15: Imaging directions: axial, sagittal, coronal

1.1.4 Non-invasive Navigation for the Head

Stereotaxic navigation with a head-frame is invasive and painful for the patient. The frame must be attached under local anesthesia. The next example shows a less invasive (but also less accurate) alternative for applications in neurology (Fig. 1.16). In transcranial magnetic stimulation (TMS), a magnetic coil stimulates small regions in the brain. For diagnostic applications, the coil is held by the surgeon. This becomes difficult if the coil must remain in the same place (with respect to the head) for extended periods of time in certain cases more than 30 min. In robotic TMS, we navigate the coil with a robot.

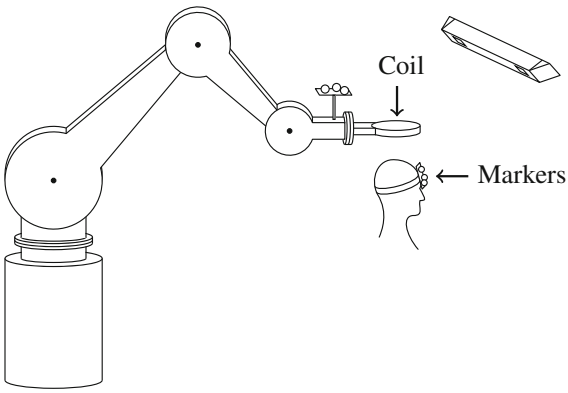

Fig. 1.16: Navigated transcranial stimulation

Surface points on the head are acquired with a marker of the infrared tracking system. An additional infrared marker is attached to the head with a velcro band. Before treatment, a second set of surface points can be computed from an MR-image. The two point sets are then matched in a registration step. In this way, we can locate a target inside the brain, given in MR-coordinates. During the procedure, the robot can compensate for small motions of the head.
Beyond the fields mentioned above (orthopedic surgery, neurosurgery and neurology), navigation methods are used in many other fields (e.g. ENT surgery, radiosurgery, abdominal surgery and heart surgery). The applications described above are simpler than many others, because the target does not deform.

1.1.5 Navigation for Moving Targets

In radiosurgery, robots are used to move the radiation source. This source weighs 200 kg and cannot be moved by the surgeon. Lung tumors move as the patient breathes. The robot compensates for this motion, i.e. the robot tracks the tumor motion, see Fig. 1.17.
Real-time tracking of internal organs is difficult, especially in this application. Methods for *motion correlation* can overcome this problem: suppose that the skin of the patient moves with respiration, and the target tumor also moves with respiration. The skin motion may be small (i.e. in a range of 1–2 mm), but we can track it with fast cameras or infrared tracking. Now assume the observable skin motion of the patient correlates to the tumor motion. Then we can use skin motion as a surrogate signal, to track the internal target.

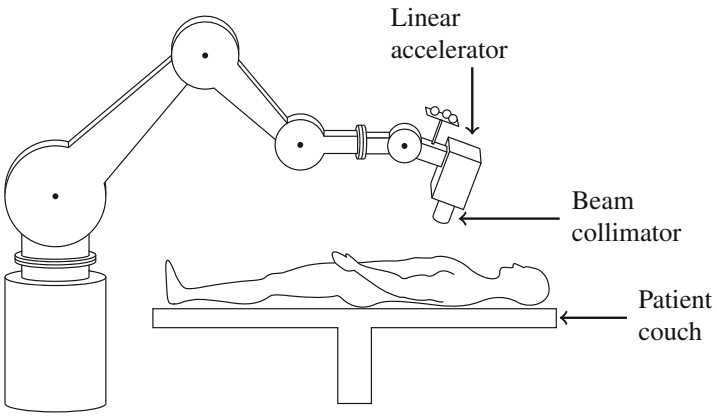

Fig. 1.17: Radiosurgery: a robotic arm or a jointed mechanism moves a medical linear accelerator. The linear accelerator generates a beam of photon radiation

In the same application (robotic radiosurgery), the motion of the robot must be planned. The plan must take into account the geometry and location relationships in the area surrounding the tumor. Hence, planning must be done on an individual basis for each treatment.

1.2 Movement Replication

As noted above, robots are not only used for navigation. Using appropriate sensors, it is not difficult to record all hand motions of a surgeon during an intervention. One can then replicate hand motion by a robotic arm. With this, a number of problems in microsurgery can be addressed. An example is shown in the next figure. The motion of the surgeon can be down-scaled. Assume the motion range of the surgeon's hand is 1 cm, and our robot replicates the same motion, but down-scales it to a range of 1 mm. Thus, delicate interventions can be performed with very high accuracy, see Fig. 1.18.

Fig. 1.18: Replicating the surgeon's hand motion with a robotic interface mounted to the patient couch (da Vinci Surgical System, ©2015 Intuitive Surgical, Inc.)

A second example is the placement of heart catheters [1]. The surgeon pushes the catheter through the blood vessel tree under image guidance. A robotic interface transmits motion commands to the tip of the catheter. The catheter tip is articulated, and can thus be steered.

1.3 Robots for Imaging

A further application of medical robots is image acquisition. The process of computing a CT image from a set of X-ray images is one instance of *image reconstruction* (see Fig. 1.19). As an example, we can move the C-shaped structure of the C-arm. Then the source-detector assembly will move along a circular arc in space. By taking a series of X-ray images during this circular motion (Fig. 1.20), we obtain the raw data for a three-dimensional CT image. A reconstruction algorithm then computes the 3D image.

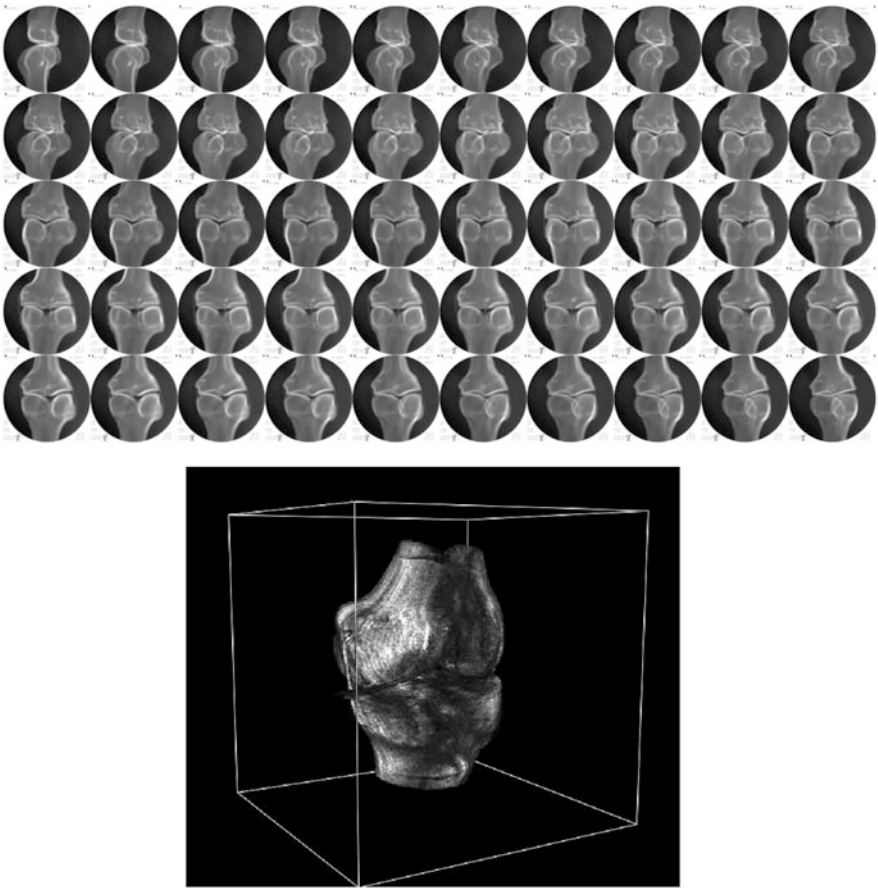

Fig. 1.19: Reconstruction. *Top*: 2D projection images taken from a series of angles. *Bottom*: Reconstructed 3D image

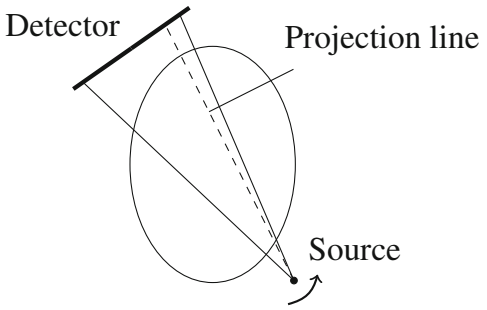

Fig. 1.20: Rotating source-detector assembly for CT imaging or 3D imaging with a C-arm

Above we discussed radiologic navigation. We saw that it combines X-ray imaging and CT imaging. Image reconstruction is closely related to navigation, since our intra-operative reconstruction may rely on partial or modified image data.
In a further application, we replace the C-arm by a robot moving the source and the detector (Fig. 1.21).
Similar to C-arms, surgical microscopes for neurosurgery and ophthalmology are mounted to jointed mechanisms (Fig. 1.22). Repositioning the microscope during the operation, even by a few millimeters, forces the surgeon to interrupt the operation. The surgeon must first hand the instruments to an assistant, then unlock the microscope's brakes and reposition the microscope manually. Then the assistant must give the instruments back to the surgeon, and the instruments are reinserted into the operation cavity. If the microscope is actuated, several of these steps become unnecessary. This not only saves operation time, but reduces infection risk.

1.4 Rehabilitation and Prosthetics

After initial rehabilitation, most stroke patients are released to daily life, often without regaining their original mobility. To improve this situation, small and simple robotic training devices have been developed. Stroke patients can use these robots at home. The robots perform simple and repetitive movements to help the patient regain mobility.

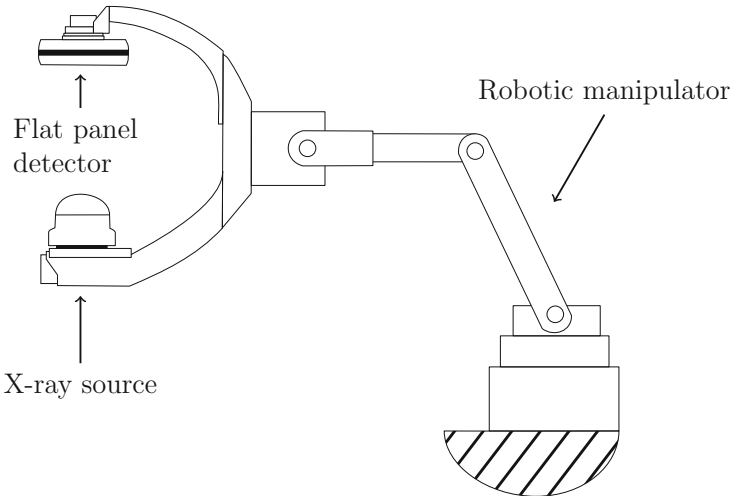

Fig. 1.21: Robotic C-arm imaging system for angiography [4]

In neuro-prosthetics, intelligent actuator systems directly assist patients in performing motion tasks, e.g. after paralysis (see Fig. 1.23). The systems can be reconfigured for various tasks, such as finger turning operations, bottle opening and grasping. In each case, the patient applies forces and torques, which can be measured to adjust the system parameters.

An exoskeleton is an external skeleton supporting the body. A first application is to reduce tremor during microsurgery. A major research goal is to provide actuated exoskeletons for paralyzed patients.

Targeted muscle reinnervation (TMR) is a surgical procedure for establishing a control channel between the patient and an exoskeleton. In TMR, several independent nerve-muscle units are created in the chest. These units can then be used for signal recording with external electromyography (EMG). EMG is non-invasive, and electrodes on the skin surface record signals from muscle contractions. With TMR, patients can control a robotic arm prosthesis. With the artificial arms, patients who lost both arms in accidents are able to perform a variety of tasks such as eating, putting on glasses and using a pair of scissors [5]. Methods from machine learning can be applied to improve the motion patterns on the side of the robot arm.

Fig. 1.22: Surgical microscope (MÖLLER 20-1000, Möller-Wedel GmbH)

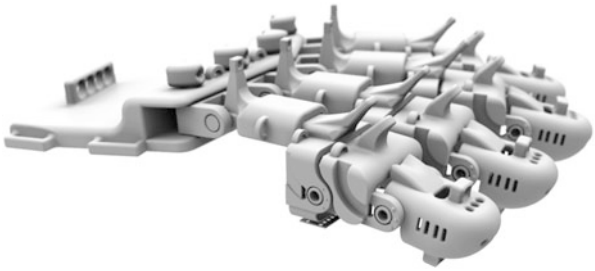

Fig. 1.23: Robotic hand for stroke rehabilitation [8]

Exercises

Exercise 1.1

The joint angles (θ_4 and θ_5) for the neurosurgical frame in Fig. 1.13 are shown in Figs. 1.24 and 1.25.

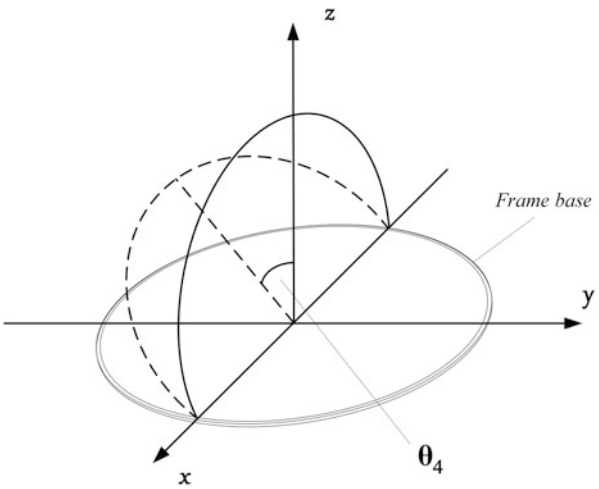

Fig. 1.24: Joint angle θ_4 for the neurosurgical frame in Fig. 1.13

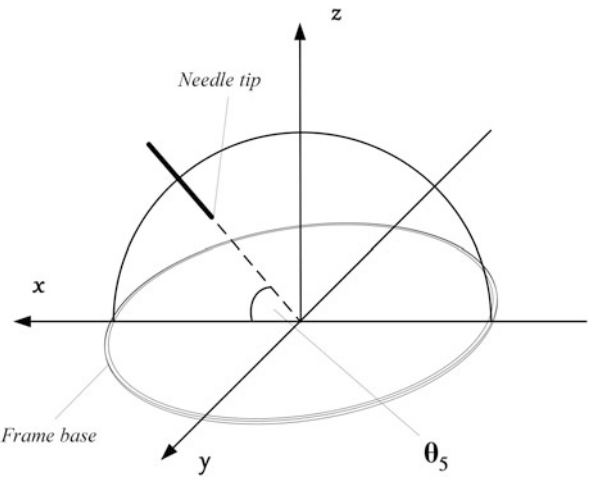

Fig. 1.25: Joint angle θ_5 for the frame in Fig. 1.13

Place a coordinate system at the centroid of the frame base, with axes (x-,y-,z-) as shown in Fig. 1.25.
Assume the distance of the needle tip (Fig. 1.25) from the coordinate origin is 100 mm.

a) For angle values taken from the set $\theta_4 \in \{-90, 0, 90\}$ and $\theta_5 \in \{0, 90, 180\}$verify that the expression

$$100 \cdot \begin{pmatrix} \cos(\theta_5) \\ -\sin(\theta_4)\sin(\theta_5) \\ \cos(\theta_4)\sin(\theta_5) \end{pmatrix} \tag{1.1}$$

gives the coordinates of the needle tip in mm.

b) Given the coordinates

$$\mathbf{p} = \begin{pmatrix} p_x \\ p_y \\ p_z \end{pmatrix} \tag{1.2}$$

of a point in space, compute the joint angles θ_4 and θ_5 for reaching this point.
Hint: Assume $\|\mathbf{p}\| = 100$. Start from the equation

$$\begin{pmatrix} p_x \\ p_y \\ p_z \end{pmatrix} = 100 \cdot \begin{pmatrix} \cos(\theta_5) \\ -\sin(\theta_4)\sin(\theta_5) \\ \cos(\theta_4)\sin(\theta_5) \end{pmatrix} \tag{1.3}$$

The first line of Eq. 1.3 gives

$$p_x = 100 \cdot \cos(\theta_5) \tag{1.4}$$

Solve this equation with the arccos-function. Then insert the solution into either of the remaining equations

$$p_y = -100 \cdot \sin(\theta_4)\sin(\theta_5) \tag{1.5}$$

and

$$p_z = 100 \cdot \cos(\theta_4)\sin(\theta_5) \tag{1.6}$$

Discuss the case $\theta_5 = 0$.

c) Discuss the case $\|\mathbf{p}\| \neq 100$ with the prismatic joints in Fig. 1.13.